

Article

Significantly Improved Colossal Dielectric Properties and Maxwell—Wagner Relaxation of TiO₂—Rich Na_{1/2}Y_{1/2}Cu₃Ti_{4+x}O₁₂ Ceramics

Pariwat Saengvong ¹, Narong Chanlek ², Bundit Putasaeng ³, Atip Pengpad ^{1,4}, Viyada Harnchana ^{1,4} , Sriprajak Krongasuk ^{1,4}, Pornjuk Srepusharawoot ^{1,4} and Prasit Thongbai ^{1,4,*} 

¹ Giant Dielectric and Computational Design Research Group (GD—CDR), Department of Physics, Faculty of Science, Khon Kaen University, Khon Kaen 40002, Thailand; mute1987@gmail.com (P.S.); atippe@kku.ac.th (A.P.); viyada@kku.ac.th (V.H.); srikro@kku.ac.th (S.K.); spornj@kku.ac.th (P.S.)

² Synchrotron Light Research Institute (Public Organization), 111 University Avenue, Muang District, Nakhon Ratchasima 30000, Thailand; narong@slri.or.th

³ National Metal and Materials Technology Center, National Science and Technology Development Agency, Thailand Science Park, Pathum Thani 12120, Thailand; bunditp@mtec.or.th

⁴ Institute of Nanomaterials Research and Innovation for Energy (IN—RIE), Khon Kaen University, Khon Kaen 40002, Thailand

* Correspondence: pthongbai@kku.ac.th



Citation: Saengvong, P.; Chanlek, N.; Putasaeng, B.; Pengpad, A.; Harnchana, V.; Krongasuk, S.; Srepusharawoot, P.; Thongbai, P. Significantly Improved Colossal Dielectric Properties and Maxwell—Wagner Relaxation of TiO₂—Rich Na_{1/2}Y_{1/2}Cu₃Ti_{4+x}O₁₂ Ceramics. *Molecules* **2021**, *26*, 6043. <https://doi.org/10.3390/molecules26196043>

Academic Editors: Giuseppe Cirillo and Hom Nath Dhakal

Received: 7 September 2021

Accepted: 30 September 2021

Published: 5 October 2021

Publisher's Note: MDPI stays neutral with regard to jurisdictional claims in published maps and institutional affiliations.



Copyright: © 2021 by the authors. Licensee MDPI, Basel, Switzerland. This article is an open access article distributed under the terms and conditions of the Creative Commons Attribution (CC BY) license (<https://creativecommons.org/licenses/by/4.0/>).

Abstract: In this work, the colossal dielectric properties and Maxwell—Wagner relaxation of TiO₂—rich Na_{1/2}Y_{1/2}Cu₃Ti_{4+x}O₁₂ ($x = 0–0.2$) ceramics prepared by a solid-state reaction method are investigated. A single phase of Na_{1/2}Y_{1/2}Cu₃Ti₄O₁₂ is achieved without the detection of any impurity phase. The highly dense microstructure is obtained, and the mean grain size is significantly reduced by a factor of 10 by increasing Ti molar ratio, resulting in an increased grain boundary density and hence grain boundary resistance (R_{gb}). The colossal permittivities of $\epsilon' \sim 0.7–1.4 \times 10^4$ with slightly dependent on frequency in the frequency range of $10^2–10^6$ Hz are obtained in the TiO₂—rich Na_{1/2}Y_{1/2}Cu₃Ti_{4+x}O₁₂ ceramics, while the dielectric loss tangent is reduced to $\tan\delta \sim 0.016–0.020$ at 1 kHz due to the increased R_{gb} . The semiconducting grain resistance (R_g) of the Na_{1/2}Y_{1/2}Cu₃Ti_{4+x}O₁₂ ceramics increases with increasing x , corresponding to the decrease in Cu⁺/Cu²⁺ ratio. The nonlinear electrical properties of the TiO₂—rich Na_{1/2}Y_{1/2}Cu₃Ti_{4+x}O₁₂ ceramics can also be improved. The colossal dielectric and nonlinear electrical properties of the TiO₂—rich Na_{1/2}Y_{1/2}Cu₃Ti_{4+x}O₁₂ ceramics are explained by the Maxwell—Wagner relaxation model based on the formation of the Schottky barrier at the grain boundary.

Keywords: colossal/giant dielectric properties; X—ray photoelectron spectroscopy; Maxwell—Wagner relaxation; impedance spectroscopy; NYCTO

1. Introduction

Improvement of electronic device efficiency through the development of materials with enhanced electrical properties is significant. Colossal dielectric oxides (CDOs) with very high dielectric constant (ϵ') are widely used to manufacture critical components in electronic devices, especially for multilayer ceramic capacitors (MLCCs) [1–3]. The ϵ' of a CDO influences the geometry and performance of the MLCCs. The size of an MLCC can be miniaturized by using the insulating oxide between the metallic electrodes with a dielectric oxide with a higher ϵ' value than the conventional oxide. Many CDOs have intensively been investigated, especially for CaCu₃Ti₄O₁₂ (CCTO) and related compounds, expecting to replace traditional CDOs such as BaTiO₃—based ceramics.

The dielectric and electrical properties of the perovskite CCTO ceramics have been extensively studied over the past two decades [4–12]. This is because CCTO ceramics showed high $\epsilon' \sim 10^3–10^5$ over wide ranges of temperature and frequency. Moreover, the ϵ'

of CCTO ceramics are relatively stable in the temperature range of 100–400 K compared to conventional BaTiO₃-based ceramics used. Unfortunately, CCTO still presents too high dielectric loss ($\tan\delta \gg 0.05$), which is not required for application in MLCCs [13–15]. Therefore, researchers have studied reducing the $\tan\delta$ of CCTO ceramics by tuning the ceramic microstructure of CCTO and related ceramics according to their heterogeneous electrical structure. The special microstructure, which consists of semiconducting grains and highly resistive boundaries (GBs), can be produced using one-step processing method [5]. This heterogeneous microstructure is called to be an internal barrier layer capacitor (IBLC) structure. Accordingly, the resistivity and correlated $\tan\delta$ can be improved by engineering the grains and GBs [16,17]. In addition, the presence of insulating GBs affects a nonlinear relationship between current density (J) and electrical field strength (E), which is a behavior required for developing varistor devices [4,9,18].

To improve the colossal dielectric and nonlinear J - E properties, many effective methods have been proposed and studied, such as doping with suitable ions [19–22], tuning ceramic microstructure [9] and fabricated CCTO-matrix composites [10,18,23,24]. These methods have the same approach, which is to increase the total resistance of the insulating GBs (R_{gb}) for reducing $\tan\delta$. One of the most effective methods is to fabricate the CCTO-matrix composites using an appropriate ceramic filler such as CaTiO₃ (CTO), Al₂O₃ or TiO₂ [6,7,10,18,25]. For the CTO/CCTO/and TiO₂/CCTO composites, although the $\tan\delta$ can be significantly reduced to <0.05 , their ϵ' values are usually significantly decreased in the order of 10^3 . For these two composite systems, the nonlinear electrical properties can also be significantly improved. The TiO₂/CCTO composites can be easily prepared by designing TiO₂-rich phase in the CCTO ceramics using the formula $\text{CaCu}_3\text{Ti}_{4+x}\text{O}_{12+2x}$. Notably, the mean grain size was reduced, resulting in a significant increase in R_{gb} . This is the primary cause of the observed improvement of the colossal dielectric and nonlinear electrical properties of CCTO ceramics.

In addition to CCTO ceramics, the colossal dielectric properties of $\text{ACu}_3\text{Ti}_4\text{O}_{12}$ oxides ($A = \text{Na}_{1/2}\text{Bi}_{1/2}$ [26], $\text{Na}_{1/2}\text{Y}_{1/2}$ [27–30], $\text{Na}_{1/2}\text{La}_{1/2}$ [31], $\text{Bi}_{2/3}$ [32,33], $\text{Y}_{2/3}$ [32,34], Cd [16,17,35], $\text{La}_{2/3}$ [32], $\text{Sm}_{2/3}$ [36], $\text{Na}_{1/3}\text{Ca}_{1/3}\text{Bi}_{1/3}$ [37], $\text{Na}_{1/3}\text{Cd}_{1/3}\text{Y}_{1/3}$ [38], $\text{Na}_{1/3}\text{Sr}_{1/3}\text{Y}_{1/3}$ [39] and $\text{Na}_{1/2}\text{Sm}_{1/2}$ [40]) are very attractive, especially for the $\text{Na}_{1/2}\text{Y}_{1/2}\text{Cu}_3\text{Ti}_4\text{O}_{12}$ (NYCTO) ceramics [27–30]. The NYCTO ceramics exhibited a high $\epsilon' \sim 10^4$ with low $\tan\delta < 0.05$ at 1 kHz compared to that of the CCTO ceramics [28–30]. Recently, the preparation, colossal dielectric permittivity and nonlinear electrical properties of NYCTO ceramics has been widely reported [27–30,39,41–43].

In this work, the TiO₂-rich NYCTO ceramics were prepared by a conventional mixed-oxide method and investigated the dielectric properties. The crystal structure, phase composition and microstructural evolution of the sintered ceramics, as well as their oxidation states, were characterized. The primary cause of the enhanced colossal dielectric response was systematically elucidated. This study contributes an exciting concept for improving the colossal dielectric properties of the NYCTO ceramics by reducing their $\tan\delta$. We believe that this research work provides an effective route to improve the CDOs for future applications in MLCCs.

2. Experimental Details

TiO₂-rich $\text{Na}_{1/2}\text{Y}_{1/2}\text{Cu}_3\text{Ti}_{4+x}\text{O}_{12}$ (NYCTO+xTiO₂) ceramics (where $x = 0.0, 0.1$ and 0.2) were prepared using solid-state reaction method (SSR). The starting materials were Na₂CO₃ (99.9%), Y₂O₃ (99.99%), CuO (99.9%) and TiO₂ (99.9%), which were purchased from Sigma-Aldrich (St. Louis, MO, USA). Details for the preparation of NYCTO-based oxides were provided elsewhere [28,30,39]. The mixed powders for all compositions were calcined at 1000 °C for 10 h. Mixed powders (without calcination) were pressed into 9.5-mm-diameter pellets by uniaxial compression at ~ 100 MPa. Finally, the pellets were sintered at 1070 °C for 10 h in air. The sintered NYCTO + xTiO₂ ceramics with $x = 0.0, 0.1$ and 0.2 were referred to as the NYCTO, NYCTO + 0.1TiO₂ and NYCTO + 0.2TiO₂, respectively.

The crystal structures of the sintered sample were characterized using X-ray diffraction (XRD, PANalytical, EMPYREAN, Shanghai, China), scanning electron microscopy (MiniSEM, SEC, SNE-4500 M), field emission scanning electron microscopy (FIB-FESEM), with energy dispersive X-ray (EDX) spectroscopy and X-ray photoemission spectroscopy (XPS, PHI5000 Versarobe II, ULVAC-PHI, Chigasaki, Japan). Comprehensive details were provided in our previous works [12,21,44–46].

For the nonlinear electrical and dielectric measurements, the surfaces of samples were polished. Next, the parallel and smooth surfaces were coated with silver paints and fired in the air at 600 °C for 30 min. The impedance and dielectric parameters of all sintered ceramics were measured with an impedance analyzer (KEYSIGHT E4990A, Santa Rosa, CA, USA). The dielectric properties were measured in the temperature range of –160 to 210 °C and the frequency range from 10^2 – 10^7 Hz. The nonlinear relationship between current density (J) and electrical field strength (E) was analyzed by using a high-voltage measurement unit (Keithley 247 model, Cleveland, OH, USA).

3. Results and Discussion

The XRD patterns of the sintered NYCTO + $x\text{TiO}_2$ ($x = 0, 0.1$ and 0.2) ceramics are illustrated in Figure 1a, showing the single phase of NYCTO in all ceramics with a perovskite-structure (JCPDS 75–2188). The crystal structure of NYCTO is demonstrated in Figure 1b. The XRD peak corresponding to TiO_2 phase cannot be detected in the NYCTO + 0.1TiO_2 and NYCTO + 0.2TiO_2 ceramics, which may be due to a small amount of an excess TiO_2 molar ratio that was lower than the resolution limit of the XRD technique. Accordingly, the lattice parameters (a) can be calculated and found to be 7.383, 7.383 and 7.384 Å for the NYCTO, NYCTO + 0.1TiO_2 and NYCTO + 0.2TiO_2 ceramics, respectively. The a values are comparable to those reported in the literature [27–30]. The excess TiO_2 composition in NYCTO ceramics does not affect the lattice parameter. This result indicates that the TiO_2 -rich phase is segregated from the primary phase of NYCTO, which may exist as the TiO_2 -rich boundary. The XRD result shows that the NYCTO + $x\text{TiO}_2$ has successfully been fabricated using the SSR method.

Even though the excessive TiO_2 phase was not detected in the XRD patterns for all ceramics, the variation in compositions of the CuO and/or TiO_2 ratios in an $\text{ACu}_3\text{Ti}_4\text{O}_{12}$ compound usually affects the dielectric and electrical properties [6,10,24,45,47–49]. Thus, we first investigated the dielectric properties of the NYCTO + $x\text{TiO}_2$ ceramics at around room temperature (30 °C). The relationship between the ϵ' and frequency of the NYCTO + $x\text{TiO}_2$ ceramics is shown in Figure 2a. The ϵ' value of the NYCTO ceramic is huge (2.07×10^4 at 10^3 Hz) with a quite low $\tan\delta \sim 0.115$, which is similar to that reported in the previous works [27,28,30]. However, the ϵ' of the NYCTO ceramic is largely dependent on the frequency in a low-frequency range, which is usually owing to the dominant effect of non-Ohmic sample-electrode interface [8,15,44,50]. At 10^6 Hz, the ϵ' begins to decline due to the primary dielectric relaxation mechanism [12,19]. Interestingly, the ϵ' values of the NYCTO + 0.1TiO_2 and NYCTO + 0.2TiO_2 ceramics are more stable with frequency than that of the NYCTO ceramic. The TiO_2 -rich phase can improve the frequency dependence of the ϵ' of the NYCTO + $x\text{TiO}_2$ ceramics. The ϵ' values of the NYCTO + 0.1TiO_2 and NYCTO + 0.2TiO_2 ceramics at 30 °C and 10^3 Hz are 1.39×10^4 and 7.15×10^3 , respectively. Even though the dielectric response in the NYCTO + 0.1TiO_2 ceramic was decreased due to the excessive TiO_2 , its ϵ' value was still larger than 10^4 over the measured frequency range. The decrease in the ϵ' value of the NYCTO + $x\text{TiO}_2$ ceramics is similar to that observed in the $\text{CaCu}_3\text{Ti}_{4+x}\text{O}_{12}$ [6].

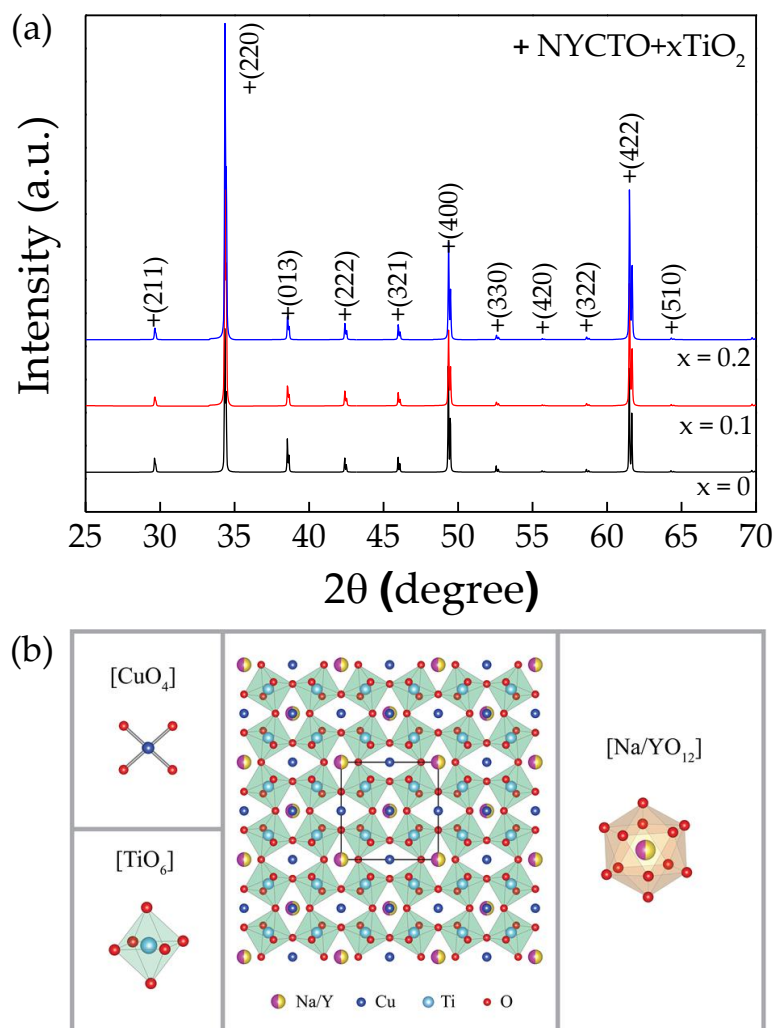


Figure 1. (a) XRD patterns of NYCTO + $x\text{TiO}_2$ ceramics with $x = 0.0, 0.1$ and 0.2 . (b) NYCTO structure.

Figure 2b illustrates the $\tan\delta$ at $30\text{ }^\circ\text{C}$ for the NYCTO + $x\text{TiO}_2$ ceramics over the frequency range of 10^2 – 10^6 Hz. In the frequency range of 10^2 – 10^5 Hz, the $\tan\delta$ values of the NYCTO + 0.1TiO_2 and NYCTO + 0.2TiO_2 ceramics are much lower than the NYCTO ceramic. Furthermore, in this frequency range, the $\tan\delta$ values of the NYCTO + 0.1TiO_2 and NYCTO + 0.2TiO_2 ceramics are lower than 0.1. The rapid increase in $\tan\delta$ of all the ceramics is attributed to the primary dielectric relaxation, i.e., Maxwell–Wagner polarization relaxation [12,19]. The $\tan\delta$ values of the NYCTO, NYCTO + 0.1TiO_2 and NYCTO + 0.2TiO_2 ceramics 10^3 Hz are 0.115, 0.020 and 0.016, respectively. Notably, the $\tan\delta$ value of the NYCTO ceramics can be significantly reduced by increasing the excessive TiO_2 -rich on the significantly improved dielectric properties of the NYCTO ceramics.

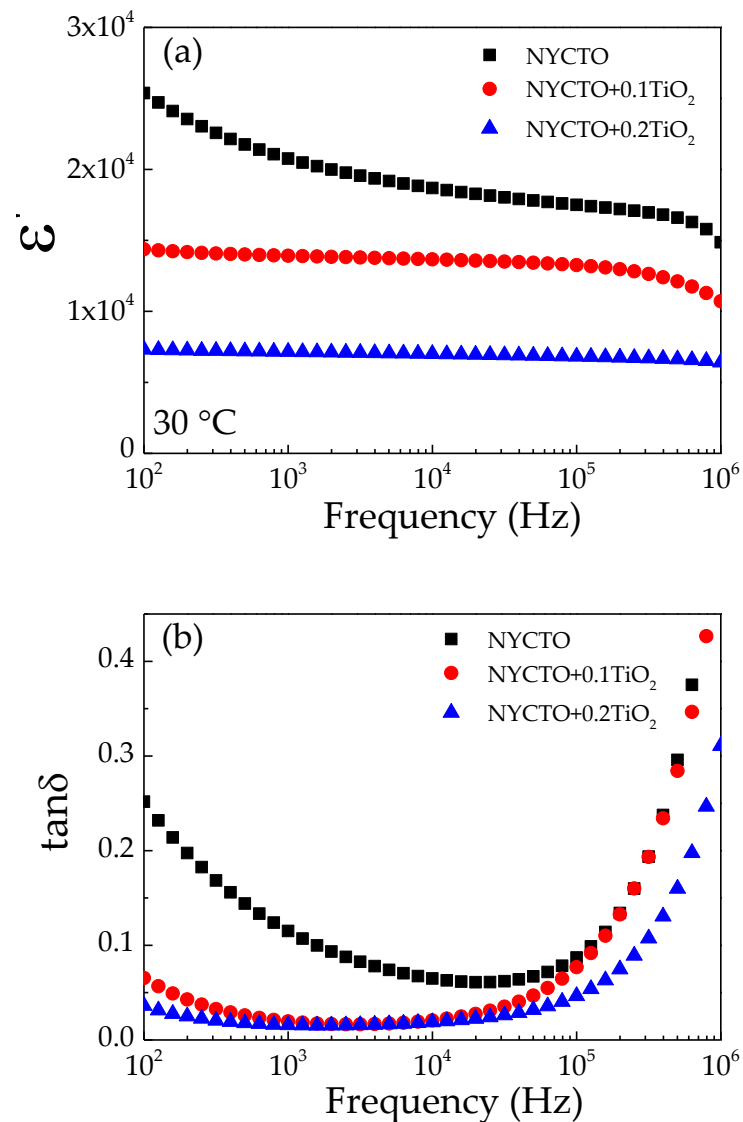


Figure 2. Dielectric properties at room temperature as a function of frequency for NYCTO + x TiO₂ ceramics with different doping content: (a) dielectric permittivity (ϵ') and (b) loss tangent ($\tan\delta$).

The temperature dependence of the dielectric properties of the NYCTO + x TiO₂ ceramics is illustrated in Figure 3a,b. In the temperature range from -125 to 110 °C, the ϵ' values of the NYCTO + 0.1TiO₂ and NYCTO + 0.2TiO₂ ceramics are more stable with temperature than that of the NYCTO ceramic. At the temperature below -120 °C, the ϵ' rapidly decreased, corresponding to the rapid increase in $\tan\delta$. This is the Maxwell—Wagner polarization relaxation in the NYCTO + x TiO₂ ceramics. Considering in the high-temperature range, the ϵ' and $\tan\delta$ significantly increase, which is associated with the DC conduction of free charge carriers associated with oxygen vacancies [11,33,51,52].

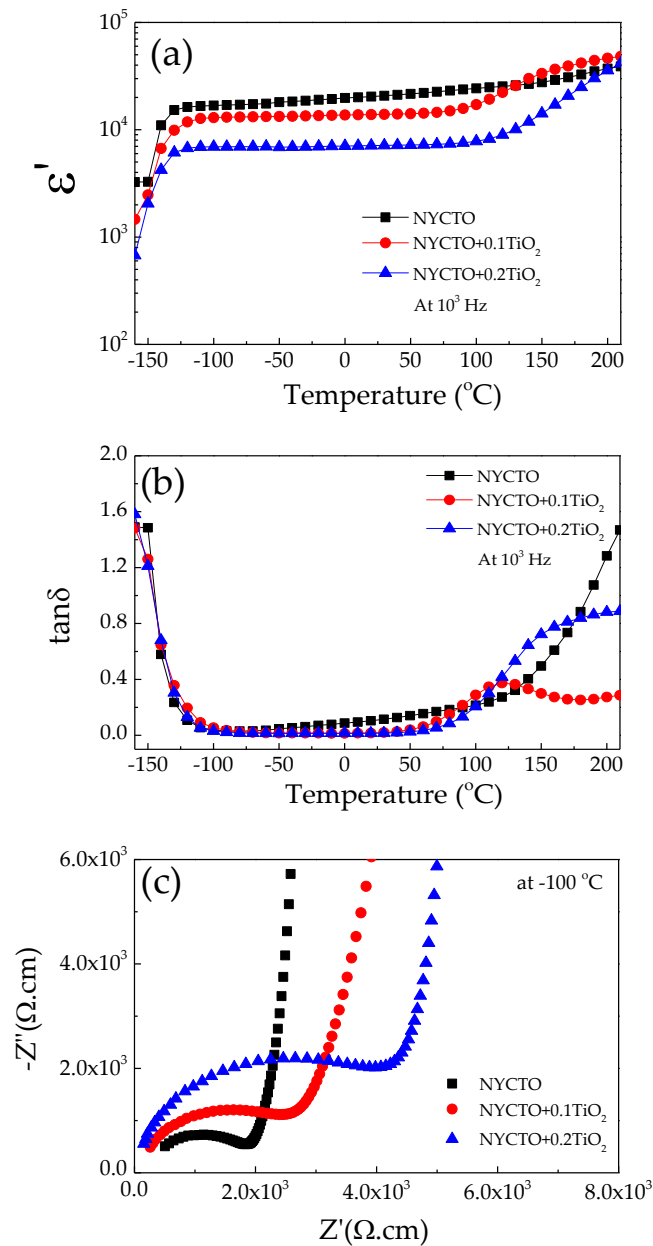


Figure 3. (a,b) Dielectric permittivity (ϵ') and loss tangent ($\tan\delta$) of NYCTO + xTiO₂ ceramics as a function of temperature (-150 – 200 °C). (c) Impedance complex plane plots (Z^*) at -100 °C, showing the electrical response on semiconducting grains.

It is widely accepted that the colossal dielectric properties of the ACu₃Ti₄O₁₂ oxide groups is the result from the electrical heterogeneous in the microstructure [5,11,15,30,33,48]. The electrically heterogeneous microstructure can be confirmed using impedance spectroscopy [5,53]. Furthermore, the heterogeneous electrical microstructure can also be used to explain the nonlinear electrical properties of the ACu₃Ti₄O₁₂ ceramics [21,23,24]. Generally, the semicircular arc due to the electrical response of the semiconducting grains of the ACu₃Ti₄O₁₂ compounds can be observed in the impedance complex plane (Z^*) plots at low temperatures [5,54]. Thus, to confirm the formation of semiconducting grains, Z^* plots of all the NYCTO + xTiO₂ ceramics are demonstrated at -100 °C, as shown in Figure 3c. The semicircular arcs of all the ceramics can be observed, while only parts of relatively large semicircular arcs can be observed. These two parts can be assigned as the electrical responses of the semiconducting grain and insulating GB, respectively [5,54].

The grain resistance (R_g), which can be calculated from the diameter of the semicircular arc of the NYCTO + $x\text{TiO}_2$ ceramics, was increased by increasing the TiO_2 molar ratio. In general, we expect that the TiO_2 —rich should not affect the electrical properties of the semiconducting grains but should only affect the insulating boundaries due to the segregation of the TiO_2 —rich phase. In this current study, the excessive TiO_2 molar ratio can affect the electrical properties inside the semiconducting grains, which will be discussed in the last section. Nevertheless, according to the impedance spectroscopy, the variation in the colossal dielectric properties and dielectric behavior of the NYCTO + $x\text{TiO}_2$ ceramics should be described in all aspects based on the IBLC model.

Figure 4a displays the Z^* plots of all the ceramics at 30 °C. Only parts of the relatively large arcs can be observed with a nonzero intercept (inset of Figure 4a), which is similar to that reported in the previous works [5,6,12,19,21,44,54]. The R_g value at 30 °C, which can be calculated from the nonzero intercept, increases with increasing the excessive TiO_2 molar ratio. Even though an entire arc cannot be observed, the R_{gb} values of all the NYCTO + $x\text{TiO}_2$ ceramics can be estimated. As shown in Figure 4b, the $\tan\delta$ of the NYCTO + $x\text{TiO}_2$ ceramics is inversely proportional to the R_{gb} value. According to the IBLC structure [20,44], the low—frequency $\tan\delta$ value is correlated to the total resistance, which is governed by the R_{gb} value. The low—frequency $\tan\delta$ can be reduced by increasing R_{gb} . Thus, the correlation of the $\tan\delta$ and R_{gb} values follows the IBLC model.

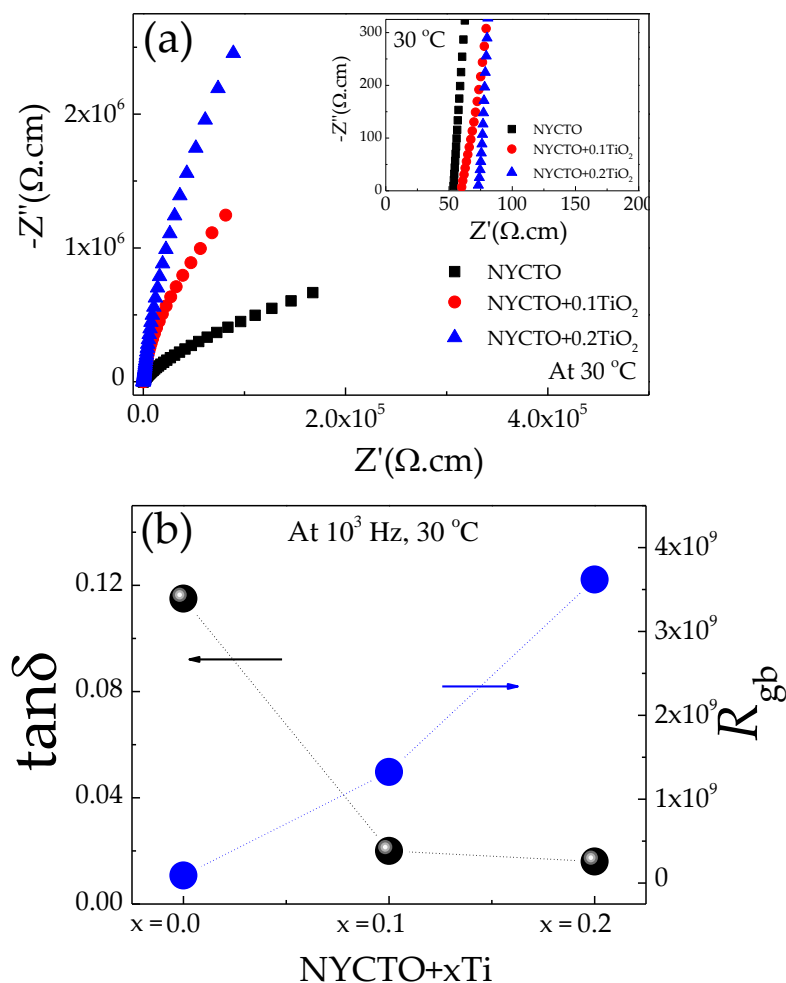


Figure 4. (a) Impedance complex plane (Z^*) plots of NYCTO + $x\text{TiO}_2$ ceramics at 30 °C; inset shows the enlarged view near the origin, showing a nonzero intercept. (b) Relationship of loss tangent ($\tan\delta$) at 1 kHz and 30 °C and grain boundary resistance (R_{gb}) at 30 °C.

In addition to the variation in $\tan\delta$, the IBLC model should be used to reasonably describe the overall dielectric properties of the NYCTO + $x\text{TiO}_2$ ceramics. Therefore, the microstructure of the sintered ceramics was studied. Figure 5 shows the SEM images of the polished surface of the NYCTO + $x\text{TiO}_2$ ceramics and their grain size distributions. All the ceramics reveal the grain and GB structure with a highly dense microstructure. The mean grain size of the NYCTO + $x\text{TiO}_2$ ceramics was extremely reduced by increasing x from 0 to 0.2. This result is similar to that reported in the previous reports for TiO_2 -rich CCTO ceramics [6]. The mean grain sizes of the NYCTO + $x\text{TiO}_2$ ceramics with $x = 0, 0.1$ and 0.2 are 32.80 ± 20.44 , 4.05 ± 2.08 and 3.18 ± 1.35 μm , respectively. The excessive TiO_2 could intercept the grain growth rate of the NYCTO ceramics due to the pinning effect of excessive TiO_2 -rich phase particles during the sintering process [55]. We also found that the segregation of the Cu-rich phase is slightly observed along the grain boundaries, as remarked in the square area of Figure 5b.

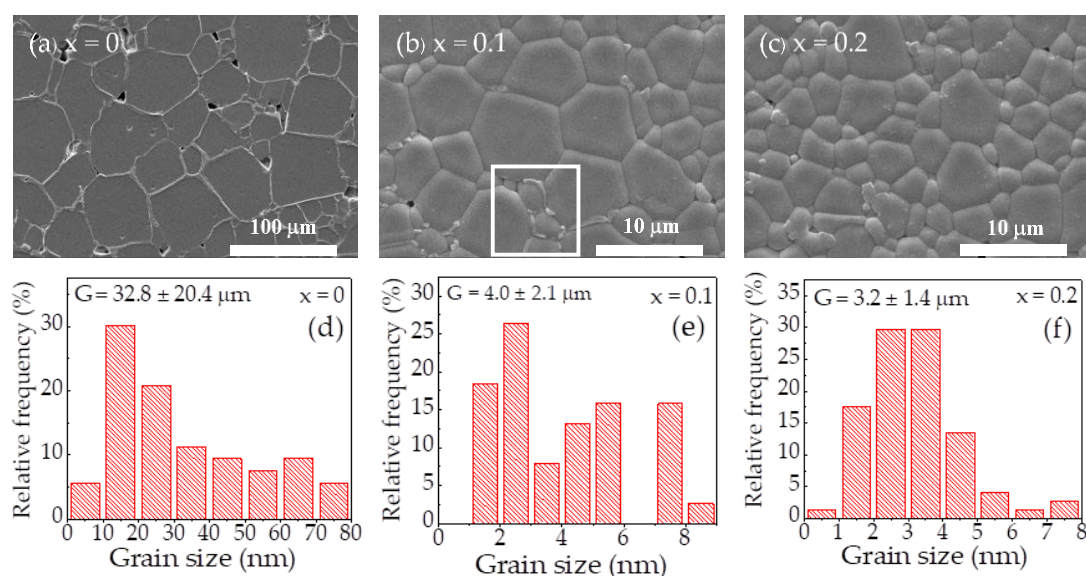


Figure 5. SEM images of NYCTO + $x\text{TiO}_2$ ceramics with $x =$ (a) 0.0, (b) 0.1 and (c) 0.2 and grain size distributions of NYCTO + $x\text{TiO}_2$ ceramics with $x =$ (d) 0.0, (e) 0.1 and (f) 0.2.

The observed decrease in ϵ' (Figure 2a) value of the NYCTO + $x\text{TiO}_2$ ceramics should be caused by the decrease in the mean grain size, following a simple series layer model of the IBLC structure [20,44,56],

$$\epsilon' = \frac{\epsilon'_{gb} G}{t_{gb}} \quad (1)$$

where G is the mean grain size, t_{gb} is the thickness of the GB and ϵ'_{gb} is the dielectric constant of the GBs. Furthermore, it is also suggested that, but does not clearly prove, the decrease in the ϵ' might be due to the increase in t_{gb} due to the TiO_2 -rich phase. The EDS and EDS-SEM mapping techniques were used to further characterize the microstructure and elemental distribution. As revealed in Figure 6a and its inset, all elements comprising the NYCTO + 0.1TiO_2 ceramic are observed in the EDS spectra, confirming the existence of Na, Y, Cu, Ti and O elements. As demonstrated in Figure 6b–g, the Na, Y, Cu and O elements disperse well throughout the microstructure. It is observed that the relatively higher brightness of Ti mapping element along the GBs compared to that of the grains can be observed, confirming the segregation of TiO_2 -rich boundary. Thus, this is one of the most important factors contributing to the decrease in the ϵ' values of the NYCTO + 0.1TiO_2 and NYCTO + 0.2TiO_2 ceramics. According to the microstructure analyses, the density of the insulating GB layers in the NYCTO + $x\text{TiO}_2$ ceramics was significantly increased by

increasing TiO_2 -rich phase owing to the decreased mean grain size [9,20]. Obviously, The significantly increased R_{gb} (Figure 4) is also attributed to the enhancement of insulating GB density. Furthermore, the increased R_{gb} is also due to the increase in t_{gb} . The XEX spectra detected at the grain and GB areas are shown in Figure 7. It was found that the percentage ratios of $\text{Ti}(\text{wt}\%)/\text{Cu}(\text{wt}\%)$ at the grain and GB were found to be 0.808 and 0.834, respectively.

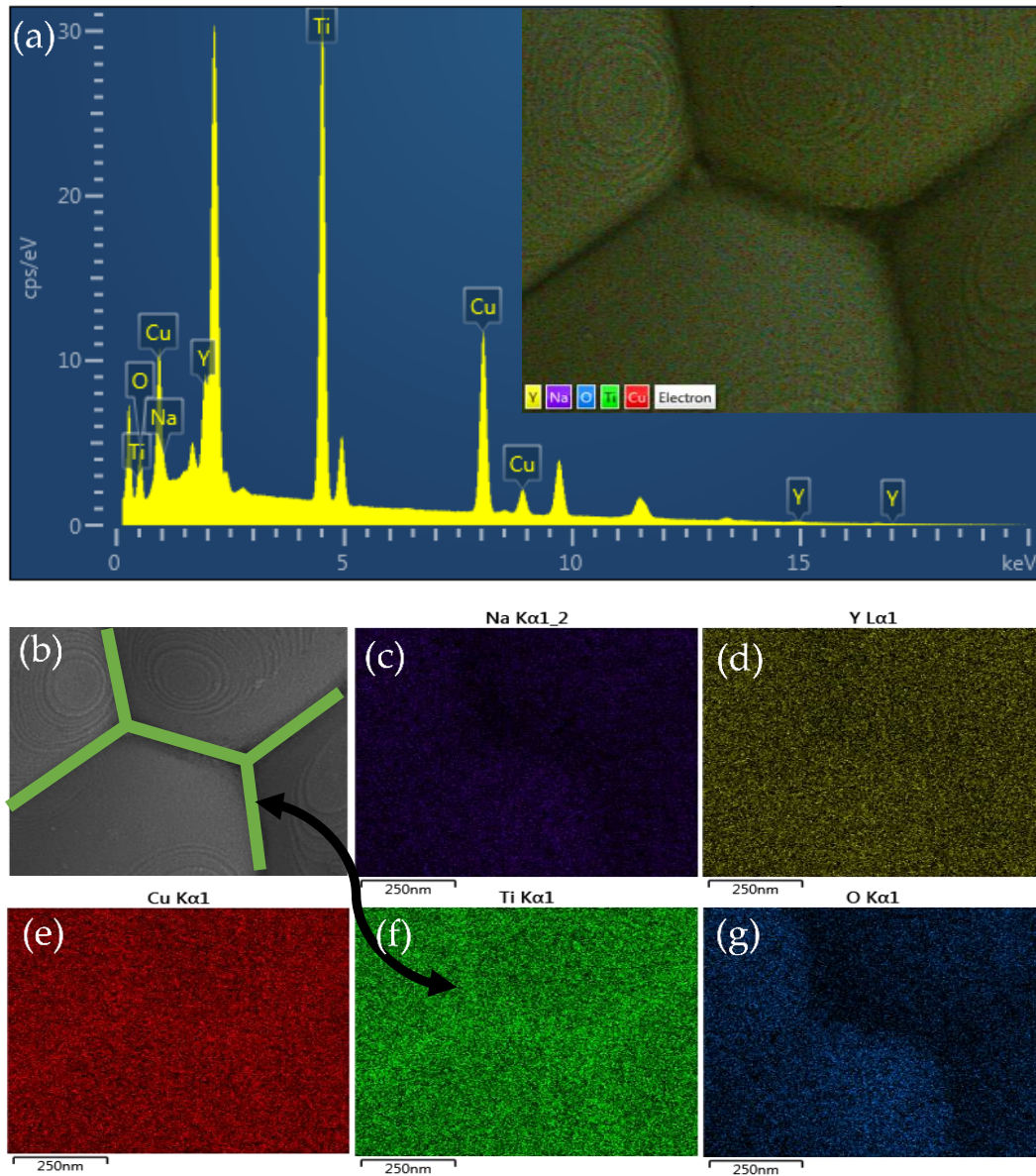


Figure 6. (a) EDS spectrum of NYCTO + $x\text{TiO}_2$ ceramic with $x = 0.1$; inset shows EDS testing area. (b) SEM image and corresponding SEM—EDS mapping images of (c) Na, (d) Y, (e) Cu, (f) Ti and (g) O for NYCTO + $x\text{TiO}_2$ ceramic with $x = 0.1$.

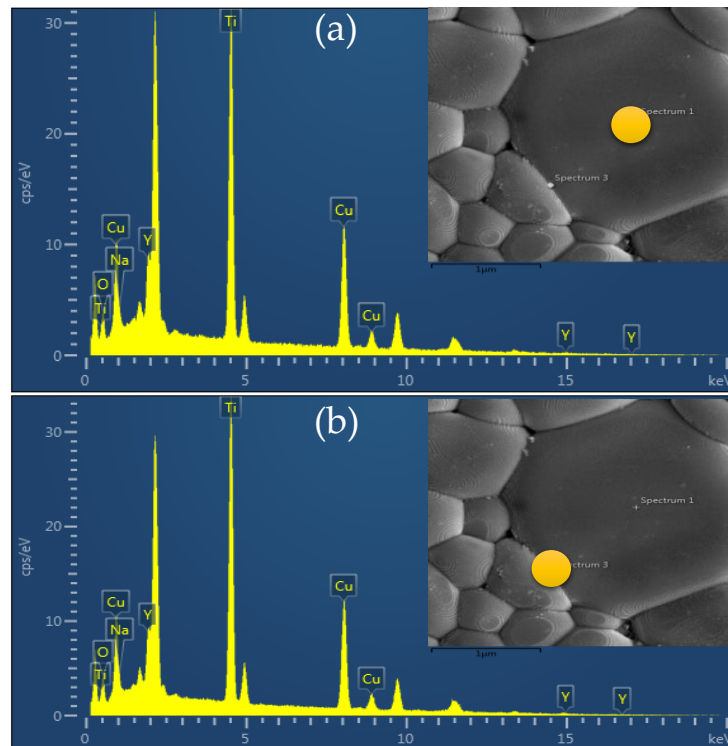


Figure 7. EDX spectra of NYCTO + $x\text{TiO}_2$ ceramic with $x = 0.2$ detected at (a) grain and (b) GB; insets show the detected points in the microstructure.

According to our previous work [28,29], it was found that the NYCTO ceramics exhibited the nonlinear J – E characteristics with nonlinear coefficients (α) of 5.7–6.6. Furthermore, it was reported that the nonlinear properties of CCTO ceramics could be enhanced by increasing the excessive TiO_2 molar ratio [6,7]. The α value of the $\text{CaCu}_3\text{Ti}_{4+x}\text{O}_{12+2x}$ ceramic with $x = 0.15$ was increased to 7.9. As illustrated in Figure 8, all the NYCTO + $x\text{TiO}_2$ ceramics exhibit the J – E characteristics. The α and electric breakdown (E_b) of the NYCTO, NYCTO + 0.1TiO_2 and NYCTO + 0.2TiO_2 ceramics are 4.96 and 724.50 V/cm, 4.71 and 910.59 V/cm, and 13.36 and 7948.04 V/cm, respectively. The E_b increased significantly with increasing TiO_2 —rich phase, similar to that observed in the $\text{CaCu}_3\text{Ti}_{4+x}\text{O}_{12+2x}$ ceramics [6]. Nevertheless, the enhanced α value of 13.36 is larger than that of the $\text{CaCu}_3\text{Ti}_{4+x}\text{O}_{12+2x}$ ceramics. The segregation of TiO_2 —rich boundary and the increased GB density are the key factors, giving rise to the significantly improved nonlinear J – E properties. The α value is often related to E_b value [4].

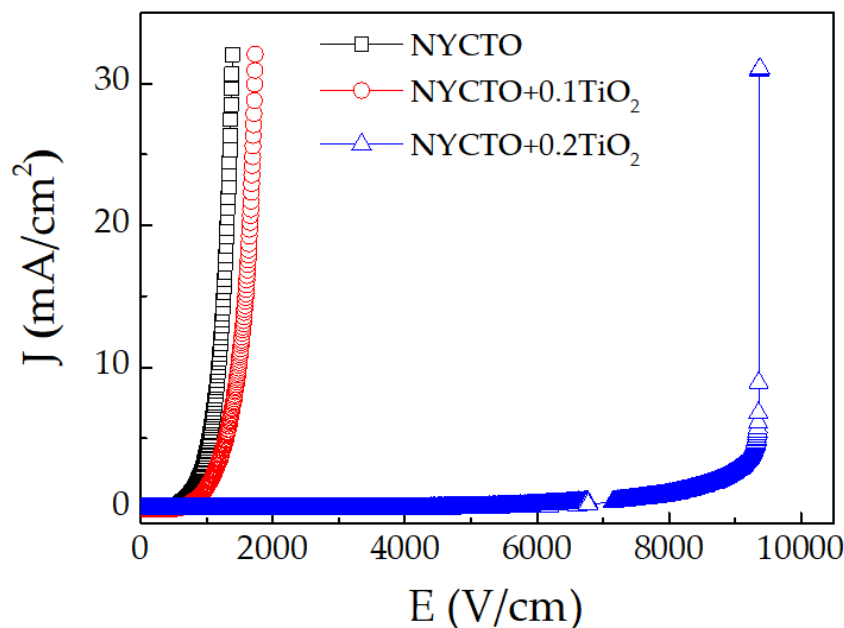


Figure 8. Nonlinear current density (J)—Electric field (E) at room temperature for NYCTO + $x\text{TiO}_2$ ceramics with $x = 0.0, 0.1$ and 0.2 .

The nonlinear electrical behavior of $\text{ACu}_3\text{Ti}_4\text{O}_{12}$ oxides is widely believed to be originated by the formation of the Schottky barrier at the GBs [4,5,7,18]. The increased E_b value is associated with the increase in R_{gb} due to the significantly increased GB density and GB thickness, which are classified as the geometric factors of the GBs [9]. Furthermore, the intrinsic factor of the GBs, i.e., the Schottky barrier height (Φ_b), can usually have a remarkable effect on the R_{gb} and E_b values [4,5,7,9]. The Φ_b is closely related to the conduction activation energy at the GBs (E_{gb}) [7,13,14]. To calculate the E_{gb} value, R_{gb} values at different temperatures were calculated. Figure 9a and its inset show Z^* plots and nonzero intercept of the NYCTO ceramic at various temperatures. The R_g and R_{gb} values can be obtained and found to decrease with increasing temperature. Thus, E_{gb} can be calculated by using the Arrhenius law [5,9]:

$$R_{gb} = R_0 \exp\left(\frac{E_{gb}}{k_B T}\right), \quad (2)$$

where R_0 , k_B and T are the pre-exponential constant term, Boltzmann constant and absolute temperature, respectively. Figure 9b depicts the relationship between R_{gb} and $1000/T$ of the NYCTO + $x\text{TiO}_2$ ceramics. The E_{gb} values can be calculated from the slopes of the R_{gb} and $1000/T$ plots, which are linearly fitted by using the Arrhenius law. The E_{gb} values of the NYCTO + $x\text{TiO}_2$ ceramics are 0.547, 0.583 and 0.714 eV, respectively. Therefore, Φ_b of the NYCTO + $x\text{TiO}_2$ ceramics can be increased by increasing the TiO_2 -rich phase. The improved nonlinear J - E properties and electrical properties of the GBs are also caused by the enhanced Φ_b , just as observed in the TiO_2 -rich CCTO ceramics [7]. The increased Φ_b values of the NYCTO + $x\text{TiO}_2$ ceramics are likely attributed to the suppressed oxygen vacancies and/or oxygen enrichment at the GBs due to the segregation of TiO_2 -rich boundary [7,18].

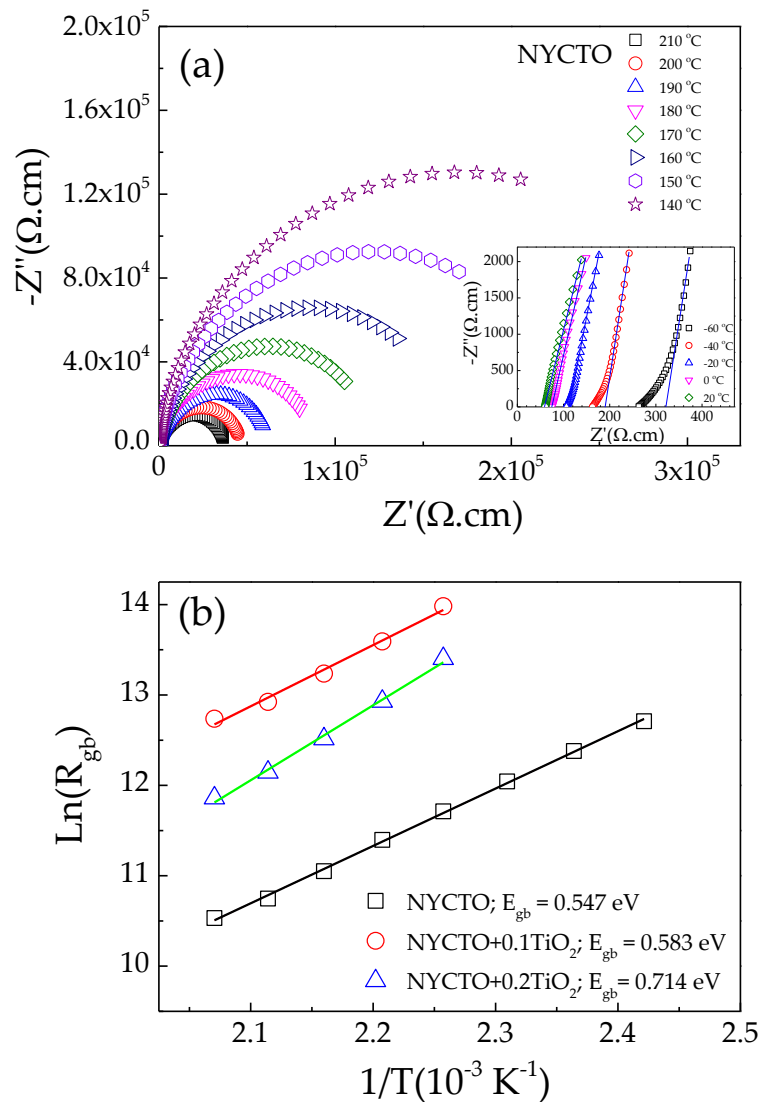


Figure 9. (a) Impedance complex plane plots (Z^*) of NYCTO ceramic at various temperature (140–210 °C). (b) Arrhenius plot for grain boundary conductivity (R_{gb}).

In addition to the electrical properties of the GBs, the electrical properties of the semiconducting grains must also be characterized. The conduction activation energy of the grains (E_g) can be calculated from the temperature dependence of R_g . The R_g values at a low-temperature range can be easily calculated using the admittance spectroscopy (Y^*) [28,29,57], as the following equation:

$$Y^* = \frac{(R_{gb}^{-1}) \left(1 - \omega^2 \tau_g \tau_{gb} + i\omega \tau_{gb} \right)}{1 + i\omega \tau}, \quad (3)$$

where $\tau_{gb} = R_{gb}C_{gb}$, $\tau_g = R_gC_g$ and $\tau = R_gC_{gb}$ and C_g and C_{gb} are the grain and GB capacitance values, respectively. According to the impedance spectroscopy, it was found that $R_{gb} \gg R_g$ and $C_{gb} \gg C_g$. From Equation (3), R_g can be obtained from the relation $R_g = 1/2Y''_{max}$, where Y''_{max} is the maximum value at Y'' peak. As shown in Figure 10a–c, Y''_{max} appears in the temperature range from -60 to 0 °C. Consequently, E_g can be calculated by using the Arrhenius law, $\sigma_g = \sigma_0 \exp(-E_g/k_bT)$, where σ_g is the grain conductivity ($\sigma_g \propto 1/R_g$), and σ_0 is a pre-exponential constant term. The E_g can be calculated by the linear fitting data, as demonstrated in the insets of Figure 10a–c. The E_g values are 0.112, 0.118 and

0.126 eV for the NYCTO, NYCTO + 0.1TiO₂ and NYCTO + 0.2TiO₂ ceramics, respectively. The E_g slightly increased with increasing the excessive TiO₂, corresponding to the increase in R_{gb} (Figure 3c). The difference between E_g and E_{gb} clearly indicates the formation of IBLC microstructure, consisting of the semiconducting grains and insulating GBs.

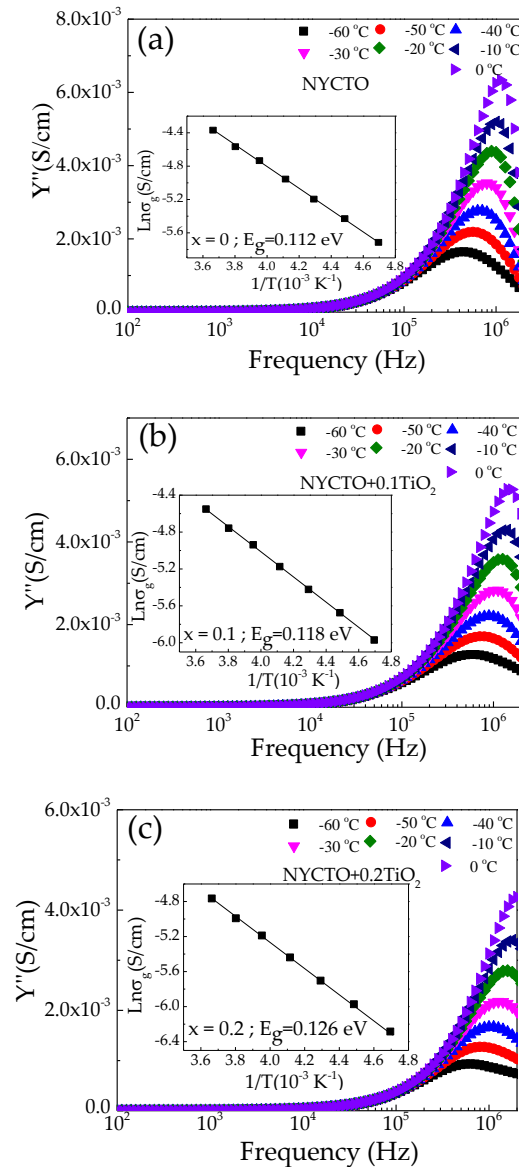


Figure 10. Imaginary part of admittance (Y'') as a function of frequency at different temperatures (−60–0 °C) for NYCTO + x TiO₂ ceramics with $x =$ (a) 0.0, (b) 0.1 and (c) 0.2; their insets show the Arrhenius plots for the grain conductivity (σ_g).

The XPS technique was further used to characterize the electrical properties of the grains. Figure 11a–c displays the XPS spectra of the Cu $2p_{3/2}$ for the NYCTO, NYCTO + 0.1TiO₂ and NYCTO + 0.2TiO₂ ceramics, respectively. According to the fitted curves, the XPS peak of the Cu $2p_{3/2}$ can be divided into two peaks at relatively low and high binding energies, corresponding to the Cu⁺ and Cu²⁺, respectively. Note that only Ti⁴⁺ can be detected in the XPS spectra, as shown in Figure 11d–f. Thus, the conduction in the semiconducting grains of all the ceramics is attributed to the electron hopping between Cu⁺ \leftrightarrow Cu²⁺. The Cu⁺/Cu²⁺ ratios of the NYCTO, NYCTO + 0.1TiO₂ and NYCTO + 0.2TiO₂ ceramics are 0.069 ± 0.027 , 0.053 ± 0.021 and 0.049 ± 0.020 , respectively. The Cu⁺/Cu²⁺ ratios decreased

with increasing TiO₂-rich phase. Generally, CCTO and related ACu₃Ti₄O₁₂ ceramics lose small amount of oxygen during sintering, giving rise to oxygen vacancies and associated free electrons [5,9]. Accordingly, a small amount of Cu⁺ and/or Ti⁴⁺ can be detected. For the NYCTO + 0.1TiO₂ and NYCTO + 0.2TiO₂ ceramics, the diffusion of oxygen vacancies during the sintering process may be inhibited by the segregation of TiO₂-rich phase along the GBs. Thus, the oxygen loss and related oxygen vacancies in the TiO₂-rich NYCTO ceramics were reduced, leading to the decrease in Cu⁺ ions. The increased R_g (Figure 3c) can be proved to be caused by the decreased Cu⁺/Cu²⁺ ratios. In addition to the grain size effect, the observed decrease in the ϵ' of the NYCTO + 0.1TiO₂ and NYCTO + 0.2TiO₂ ceramics can be described based on the IBLC microstructure. Under an applied electric field, charge carriers inside the semiconducting grains are moved to trap at the insulating GB due to a high potential barrier height, inducing the interfacial polarization and hence high ϵ' value. The intensity of the interfacial polarization of the NYCTO + 0.1TiO₂ and NYCTO + 0.2TiO₂ ceramics should be lower than that of the NYCTO ceramic because of a lower concentration of free carriers inside the grains, which is considered by a larger R_g value.

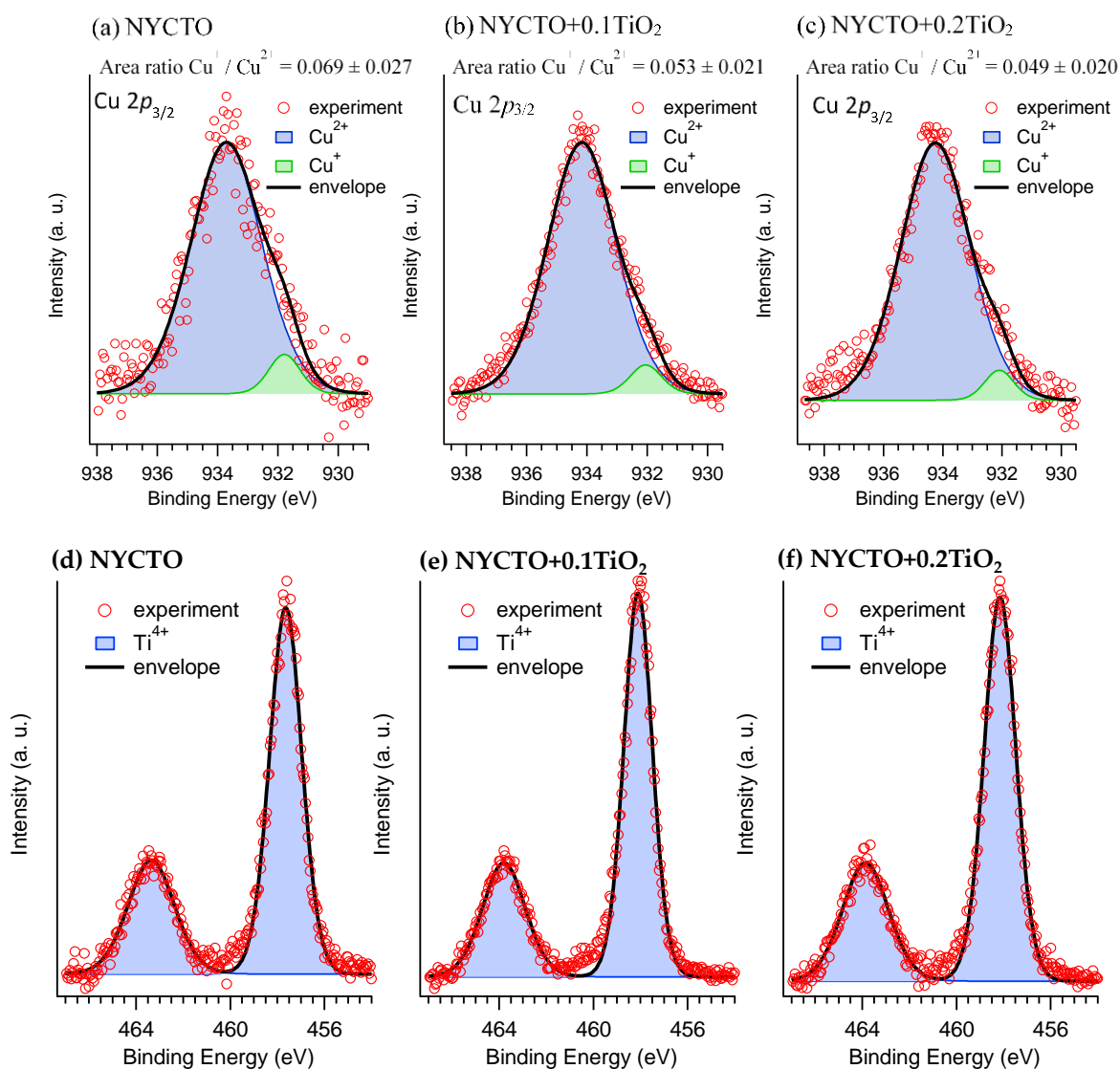


Figure 11. (a–c) XPS spectra of Cu 2p_{3/2} for all sintered NYCTO + xTiO₂ ceramics. (d–f) XPS spectra of Ti 2p for all sintered NYCTO + xTiO₂ ceramics.

4. Conclusions

In conclusion, we have successfully synthesized the TiO₂-rich NYCTO ceramics prepared using the SSR method. The effects of Ti-excess on the microstructure, colossal dielectric properties and nonlinear J - E characteristics were studied. Only the main phase of the NYCTO structure was detected in the XRD patterns, which might be due to the presence of an amorphous phase of TiO₂ along the GBs. Significantly reduced grain with highly dense microstructure was observed in the TiO₂-rich NYCTO ceramics, which was due to the pinning effect of the TiO₂-rich phase particles. The reduced grain sizes, which can cause an increase in the GB density, resulted in the significant enhancement of R_{gb} , and hence reduced $\tan\delta$. The colossal ϵ' values of ~ 0.7 – 1.4×10^4 was achieved in the TiO₂-rich NYCTO ceramics. The TiO₂-rich NYCTO ceramics also showed the enhanced nonlinear J - E properties due to the improved GB properties. The R_g value was also increased owing to the decreased Cu^+/Cu^{2+} ratio, confirming by the XPS result. The overall colossal dielectric permittivity and nonlinear electrical properties were well described using the Maxwell–Wagner polarization relaxation model based on the formation of the Schottky barrier at the grain boundary.

Author Contributions: Conceptualization, P.T.; methodology, P.S. (Pariwat Saengvong); formal analysis, P.S.(Pariwat Saengvong) and P.T.; investigation, P.S. (Pariwat Saengvong), N.C., B.P., A.P., V.H., S.K., P.S. (Pornjuk Srepusharawoot) and P.T.; writing—original draft preparation, P.S. (Pariwat Saengvong) and P.T.; writing—review and editing, P.T.; visualization, P.S. (Pariwat Saengvong) and P.T. All authors have read and agreed to the published version of the manuscript.

Funding: This project is funded by National Research Council of Thailand (NRCT) (Grant No. N41A640084). This research was also funded by the Research and Graduate Studies, Khon Kaen University.

Institutional Review Board Statement: Not applicable.

Informed Consent Statement: Not applicable.

Data Availability Statement: The data presented in this study are available in article.

Acknowledgments: This project is funded by National Research Council of Thailand (NRCT): (N41A640084). This research was also funded by the Research and Graduate Studies, Khon Kaen University. P. Saengvong expresses his gratitude to the Science Achievement Scholarship of Thailand (SAST) for a Ph.D. scholarship in Physics.

Conflicts of Interest: The authors declare no conflict of interest.

Sample Availability: Not applicable.

References

1. Wang, Y.; Jie, W.; Yang, C.; Wei, X.; Hao, J. Colossal Permittivity Materials as Superior Dielectrics for Diverse Applications. *Adv. Funct. Mater.* **2019**, *29*, 1808118. [[CrossRef](#)]
2. Zhu, J.; Wu, D.; Liang, P.; Zhou, X.; Peng, Z.; Chao, X.; Yang, Z. Ag⁺/W⁶⁺ co-doped TiO₂ ceramic with colossal permittivity and low loss. *J. Alloys. Compd.* **2021**, *856*, 157350. [[CrossRef](#)]
3. Zhou, X.; Liang, P.; Zhu, J.; Peng, Z.; Chao, X.; Yang, Z. Enhanced dielectric performance of (Ag_{1/4}Nb_{3/4})_{0.01}Ti_{0.99}O₂ ceramic prepared by a wet-chemistry method. *Ceram. Int.* **2020**, *46*, 11921–11925. [[CrossRef](#)]
4. Chung, S.-Y.; Kim, I.-D.; Kang, S.-J.L. Strong nonlinear current–voltage behaviour in perovskite-derivative calcium copper titanate. *Nat. Mater.* **2004**, *3*, 774–778. [[CrossRef](#)] [[PubMed](#)]
5. Adams, T.; Sinclair, D.; West, A. Characterization of grain boundary impedances in fine-and coarse-grained CaCu₃Ti₄O₁₂ ceramics. *Phys. Rev. B* **2006**, *73*, 094124. [[CrossRef](#)]
6. Lin, Y.-H.; Cai, J.; Li, M.; Nan, C.-W.; He, J. High dielectric and nonlinear electrical behaviors in TiO₂-rich CaCu₃Ti₄O₁₂ ceramics. *Appl. Phys. Lett.* **2006**, *88*, 172902. [[CrossRef](#)]
7. Lin, Y.-H.; Cai, J.; Li, M.; Nan, C.-W.; He, J. Grain boundary behavior in varistor-capacitor TiO₂-rich CaCu₃Ti₄O₁₂ ceramics. *J. Appl. Phys.* **2008**, *103*, 074111. [[CrossRef](#)]
8. Li, M.; Shen, Z.; Nygren, M.; Feteira, A.; Sinclair, D.C.; West, A.R. Origin(s) of the apparent high permittivity in CaCu₃Ti₄O₁₂ ceramics: Clarification on the contributions from internal barrier layer capacitor and sample-electrode contact effects. *J. Appl. Phys.* **2009**, *106*, 104106. [[CrossRef](#)]

9. Thongbai, P.; Yamwong, T.; Maensiri, S.; Amornkitbamrung, V.; Chindaprasirt, P. Improved Dielectric and Nonlinear Electrical Properties of Fine-Grained $\text{CaCu}_3\text{Ti}_4\text{O}_{12}$ Ceramics Prepared by a Glycine-Nitrate Process. *J. Am. Ceram. Soc.* **2014**, *97*, 1785–1790. [[CrossRef](#)]
10. Maleki Shahraki, M.; Daeijavad, H.; Emami, A.H.; Abdollahi, M.; Karimi, A. An engineering design based on nano/micro-sized composite for $\text{CaTiO}_3/\text{CaCu}_3\text{Ti}_4\text{O}_{12}$ materials and its dielectric and non-Ohmic properties. *Ceram. Int.* **2019**, *45*, 21676–21683. [[CrossRef](#)]
11. Kozlinskei, L.L.; de Andrade Paes, A.T.; Grzebielucka, E.C.; Borges, C.P.F.; de Andrade, A.V.C.; de Souza, E.C.F.; Antunes, S.R.M. Processing influence in the $\text{CaCu}_3\text{Ti}_4\text{O}_{12}$ electrical properties. *Appl. Phys. A* **2020**, *126*, 447. [[CrossRef](#)]
12. Jumpatam, J.; Putasaeng, B.; Chanlek, N.; Manyam, J.; Srepusharawoot, P.; Kongsuk, S.; Thongbai, P. Influence of Sn and F dopants on giant dielectric response and Schottky potential barrier at grain boundaries of CCTO ceramics. *Ceram. Int.* **2021**, *47*, 27908–27915. [[CrossRef](#)]
13. Liu, L.; Fan, H.; Fang, P.; Chen, X. Sol–gel derived $\text{CaCu}_3\text{Ti}_4\text{O}_{12}$ ceramics: Synthesis, characterization and electrical properties. *Mater. Res. Bull.* **2008**, *43*, 1800–1807. [[CrossRef](#)]
14. Jumpatam, J.; Putasaeng, B.; Yamwong, T.; Thongbai, P.; Maensiri, S. Enhancement of giant dielectric response in Ga-doped $\text{CaCu}_3\text{Ti}_4\text{O}_{12}$ ceramics. *Ceram. Int.* **2013**, *39*, 1057–1064. [[CrossRef](#)]
15. Lin, H.; Xu, W.; Zhang, H.; Chen, C.; Zhou, Y.; Yi, Z. Origin of high dielectric performance in fine grain-sized $\text{CaCu}_3\text{Ti}_4\text{O}_{12}$ materials. *J. Eur. Ceram. Soc.* **2020**, *40*, 1957–1966. [[CrossRef](#)]
16. Peng, Z.; Wang, J.; Zhou, X.; Zhu, J.; Lei, X.; Liang, P.; Chao, X.; Yang, Z. Grain engineering inducing high energy storage in $\text{CdCu}_3\text{Ti}_4\text{O}_{12}$ ceramics. *Ceram. Int.* **2020**, *46*, 14425–14430. [[CrossRef](#)]
17. Peng, Z.; Wu, D.; Liang, P.; Zhou, X.; Wang, J.; Zhu, J.; Chao, X.; Yang, Z. Grain boundary engineering that induces ultrahigh permittivity and decreased dielectric loss in $\text{CdCu}_3\text{Ti}_4\text{O}_{12}$ ceramics. *J. Am. Ceram. Soc.* **2020**, *103*, 1230–1240. [[CrossRef](#)]
18. Ramírez, M.A.; Bueno, P.R.; Varela, J.A.; Longo, E. Non-Ohmic and dielectric properties of a $\text{Ca}_2\text{Cu}_2\text{Ti}_4\text{O}_{12}$ polycrystalline system. *Appl. Phys. Lett.* **2006**, *89*, 212102. [[CrossRef](#)]
19. Boonlakhorn, J.; Manyam, J.; Srepusharawoot, P.; Kongsuk, S.; Thongbai, P. Effects of Charge Compensation on Colossal Permittivity and Electrical Properties of Grain Boundary of $\text{CaCu}_3\text{Ti}_4\text{O}_{12}$ Ceramics Substituted by Al^{3+} and $\text{Ta}^{5+}/\text{Nb}^{5+}$. *Molecules* **2021**, *26*, 3294. [[CrossRef](#)]
20. Boonlakhorn, J.; Chanlek, N.; Manyam, J.; Srepusharawoot, P.; Thongbai, P. Simultaneous two-step enhanced permittivity and reduced loss tangent in Mg/Ge-Doped $\text{CaCu}_3\text{Ti}_4\text{O}_{12}$ ceramics. *J. Alloys. Compd.* **2021**, *877*, 160322. [[CrossRef](#)]
21. Jumpatam, J.; Putasaeng, B.; Chanlek, N.; Boonlakhorn, J.; Thongbai, P.; Phromviyo, N.; Chindaprasirt, P. Significantly improving the giant dielectric properties of $\text{CaCu}_3\text{Ti}_4\text{O}_{12}$ ceramics by co-doping with Sr^{2+} and F^- ions. *Mater. Res. Bull.* **2021**, 111043. [[CrossRef](#)]
22. Boonlakhorn, J.; Putasaeng, B.; Kidkhunthod, P.; Manyam, J.; Kongsuk, S.; Srepusharawoot, P.; Thongbai, P. First-principles calculations and experimental study of enhanced nonlinear and dielectric properties of Sn^{4+} -doped $\text{CaCu}_{2.95}\text{Mg}_{0.05}\text{Ti}_4\text{O}_{12}$ ceramics. *J. Eur. Ceram. Soc.* **2021**, *41*, 5176–5183. [[CrossRef](#)]
23. Cortés, J.A.; Moreno, H.; Orrego, S.; Bezzon, V.D.N.; Ramírez, M.A. Dielectric and non-ohmic analysis of Sr^{2+} influences on $\text{CaCu}_3\text{Ti}_4\text{O}_{12}$ -based ceramic composites. *Mater. Res. Bull.* **2021**, *134*, 111071. [[CrossRef](#)]
24. Cotrim, G.; Cortés, J.A.; Moreno, H.; Freitas, S.M.; Rezende, M.V.S.; Hein, L.R.O.; Ramírez, M.A. Tunable capacitor-varistor response of $\text{CaCu}_3\text{Ti}_4\text{O}_{12}/\text{CaTiO}_3$ ceramic composites with SnO_2 addition. *Mater. Charact.* **2020**, *170*, 110699. [[CrossRef](#)]
25. Jumpatam, J.; Chanlek, N.; Thongbai, P. Giant dielectric response, electrical properties and nonlinear current-voltage characteristic of $\text{Al}_2\text{O}_3\text{-CaCu}_3\text{Ti}_4\text{O}_{12}$ nanocomposites. *Appl. Surf. Sci.* **2019**, *476*, 623–631. [[CrossRef](#)]
26. Tuichai, W.; Danwittayakul, S.; Yamwong, T.; Thongbai, P. Synthesis, dielectric properties, and influences oxygen vacancies have on electrical properties of $\text{Na}_{1/2}\text{Bi}_{1/2}\text{Cu}_3\text{Ti}_4\text{O}_{12}$ ceramics prepared by a urea combustion method. *J. Sol.-Gel Sci. Technol.* **2015**, *76*, 630–636. [[CrossRef](#)]
27. Somphan, W.; Sangwong, N.; Yamwong, T.; Thongbai, P. Giant dielectric and electrical properties of sodium yttrium copper titanate: $\text{Na}_{1/2}\text{Y}_{1/2}\text{Cu}_3\text{Ti}_4\text{O}_{12}$. *J. Mater. Sci. Mater. Electron.* **2012**, *23*, 1229–1234. [[CrossRef](#)]
28. Jumpatam, J.; Mooltang, A.; Putasaeng, B.; Kidkhunthod, P.; Chanlek, N.; Thongbai, P.; Maensiri, S. Effects of Mg^{2+} doping ions on giant dielectric properties and electrical responses of $\text{Na}_{1/2}\text{Y}_{1/2}\text{Cu}_3\text{Ti}_4\text{O}_{12}$ ceramics. *Ceram. Int.* **2016**, *42*, 16287–16295. [[CrossRef](#)]
29. Jumpatam, J.; Somphan, W.; Boonlakhorn, J.; Putasaeng, B.; Kidkhunthod, P.; Thongbai, P.; Maensiri, S. Non-Ohmic Properties and Electrical Responses of Grains and Grain Boundaries of $\text{Na}_{1/2}\text{Y}_{1/2}\text{Cu}_3\text{Ti}_4\text{O}_{12}$ Ceramics. *J. Am. Ceram. Soc.* **2017**, *100*, 157–166. [[CrossRef](#)]
30. Liang, P.; Li, Y.; Zhao, Y.; Wei, L.; Yang, Z. Origin of giant permittivity and high-temperature dielectric anomaly behavior in $\text{Na}_{0.5}\text{Y}_{0.5}\text{Cu}_3\text{Ti}_4\text{O}_{12}$ ceramics. *J. Appl. Phys.* **2013**, *113*, 224102. [[CrossRef](#)]
31. Liu, Z.; Yang, Z. Structure and electric properties of $\text{Na}_x\text{La}_{(2-x)/3}\text{Cu}_3\text{Ti}_4\text{O}_{12}$ ceramics prepared by sol–gel method. *J. Mater. Sci. Mater. Electron.* **2018**, *29*, 9326–9338. [[CrossRef](#)]
32. Liu, J.; Duan, C.-g.; Mei, W.N.; Smith, R.W.; Hardy, J.R. Dielectric properties and Maxwell-Wagner relaxation of compounds $\text{ACu}_3\text{Ti}_4\text{O}_{12}$ ($\text{A}=\text{Ca}, \text{Bi}_{2/3}, \text{Y}_{2/3}, \text{La}_{2/3}$). *J. Appl. Phys.* **2005**, *98*, 093703. [[CrossRef](#)]
33. Tang, Z.; Wu, K.; Li, J.; Huang, S. Optimized dual-function varistor-capacitor ceramics of core-shell structured $x\text{Bi}_{2/3}\text{Cu}_3\text{Ti}_4\text{O}_{12}/(1-x)\text{CaCu}_3\text{Ti}_4\text{O}_{12}$ composites. *J. Eur. Ceram. Soc.* **2020**, *40*, 3437–3444. [[CrossRef](#)]

34. Wang, X.; Liang, P.; Peng, Z.; Peng, H.; Xiang, Y.; Chao, X.; Yang, Z. Significantly enhanced breakdown electric field in Zn-doped $Y_{2/3}Cu_3Ti_4O_{12}$ ceramics. *J. Alloys. Compd.* **2019**, *778*, 391–397. [[CrossRef](#)]
35. Peng, Z.; Wang, J.; Lei, X.; Zhu, J.; Xu, S.; Liang, P.; Wei, L.; Wu, D.; Wang, J.; Chao, X.; et al. Colossal dielectric response in $CdAl_xCu_{3-x}Ti_4O_{12}$ perovskite ceramics. *Mater. Chem. Phys.* **2021**, *258*, 123940. [[CrossRef](#)]
36. Thomas, A.K.; George, M.; Abraham, K.; Sajan, D. Giant dielectric constant, dielectric relaxations, and tunable properties of $Sm_{2/3}Cu_3Ti_4O_{12}$ ceramics. *Int. J. Appl. Ceram. Technol.* **2021**, *18*, 499–510. [[CrossRef](#)]
37. Kum-onsa, P.; Thongbai, P.; Putasaeng, B.; Yamwong, T.; Maensiri, S. $Na_{1/3}Ca_{1/3}Bi_{1/3}Cu_3Ti_4O_{12}$: A new giant dielectric perovskite ceramic in $ACu_3Ti_4O_{12}$ compounds. *J. Eur. Ceram. Soc.* **2015**, *35*, 1441–1447. [[CrossRef](#)]
38. Peng, Z.; Zhou, X.; Wang, J.; Zhu, J.; Liang, P.; Chao, X.; Yang, Z. Origin of colossal permittivity and low dielectric loss in $Na_{1/3}Cd_{1/3}Y_{1/3}Cu_3Ti_4O_{12}$ ceramics. *Ceram. Int.* **2020**, *46*, 11154–11159. [[CrossRef](#)]
39. Saengvong, P.; Boonlakhorn, J.; Chanlek, N.; Putasaeng, B.; Thongbai, P. Giant dielectric permittivity with low loss tangent and excellent non-Ohmic properties of the $(Na^+, Sr^{2+}, Y^{3+})Cu_3Ti_4O_{12}$ ceramic system. *Ceram. Int.* **2020**, *46*, 9780–9785. [[CrossRef](#)]
40. Somphan, W.; Thongbai, P.; Yamwong, T.; Maensiri, S. High Schottky barrier at grain boundaries observed in $Na_{1/2}Sm_{1/2}Cu_3Ti_4O_{12}$ ceramics. *Mater. Res. Bull.* **2013**, *48*, 4087–4092. [[CrossRef](#)]
41. Kum-onsa, P.; Phromviyo, N.; Thongbai, P. Suppressing loss tangent with significantly enhanced dielectric permittivity of poly(vinylidene fluoride) by filling with $Au-Na_{1/2}Y_{1/2}Cu_3Ti_4O_{12}$ hybrid particles. *RSC* **2020**, *10*, 40442–40449. [[CrossRef](#)]
42. Kum-onsa, P.; Thongbai, P. Improved Dielectric Properties of Poly(vinylidene fluoride) Composites Incorporating $Na_{1/2}Y_{1/2}Cu_3Ti_4O_{12}$ Particles. *Mater. Today Commun.* **2020**, *25*, 101654. [[CrossRef](#)]
43. Ahmad, M.; Mahfoz Kotb, H. Giant dielectric properties of fine-grained $Na_{1/2}Y_{1/2}Cu_3Ti_4O_{12}$ ceramics prepared by mechanosynthesis and spark plasma sintering. *J. Mater. Sci. Mater. Electron.* **2015**, *26*, 8939–8948. [[CrossRef](#)]
44. Boonlakhorn, J.; Chanlek, N.; Manyam, J.; Srepusharawoot, P.; Krongsuk, S.; Thongbai, P. Enhanced giant dielectric properties and improved nonlinear electrical response in acceptor-donor (Al^{3+}, Ta^{5+}) -substituted $CaCu_3Ti_4O_{12}$ ceramics. *J. Adv. Ceram.* **2021**, *10*, 1–13.
45. Jumpatam, J.; Putasaeng, B.; Chanlek, N.; Thongbai, P. Influences of Sr^{2+} Doping on Microstructure, Giant Dielectric Behavior, and Non-Ohmic Properties of $CaCu_3Ti_4O_{12}/CaTiO_3$ Ceramic Composites. *Molecules* **2021**, *26*, 1994. [[CrossRef](#)]
46. Boonlakhorn, J.; Srepusharawoot, P.; Thongbai, P. Distinct roles between complex defect clusters and insulating grain boundary on dielectric loss behaviors of (In^{3+}/Ta^{5+}) co-doped $CaCu_3Ti_4O_{12}$ ceramics. *Results Phys.* **2020**, *16*, 102886. [[CrossRef](#)]
47. Zhao, J.; Chen, M.; Tan, Q. Embedding nanostructure and colossal permittivity of TiO_2 -covered CCTO perovskite materials by a hydrothermal route. *J. Alloys. Compd.* **2021**, *885*, 160948. [[CrossRef](#)]
48. Zhao, J.; Zhao, H.; Zhu, Z. Influence of sintering conditions and CuO loss on dielectric properties of $CaCu_3Ti_4O_{12}$ ceramics. *Mater. Res. Bull.* **2019**, *113*, 97–101. [[CrossRef](#)]
49. Gelfuso, M.V.; Uribe, J.O.M.; Thomazini, D. Deficient or excessive $CuO-TiO_2$ phase influence on dielectric properties of $CaCu_3Ti_4O_{12}$ ceramics. *Int. J. Appl. Ceram. Technol.* **2019**, *16*, 868–882. [[CrossRef](#)]
50. Mao, P.; Wang, J.; Xiao, P.; Zhang, L.; Kang, F.; Gong, H. Colossal dielectric response and relaxation behavior in novel system of Zr^{4+} and Nb^{5+} co-substituted $CaCu_3Ti_4O_{12}$ ceramics. *Ceram. Int.* **2021**, *47*, 111–120. [[CrossRef](#)]
51. Peng, Z.; Wang, J.; Liang, P.; Zhu, J.; Zhou, X.; Chao, X.; Yang, Z. A new perovskite-related ceramic with colossal permittivity and low dielectric loss. *J. Eur. Ceram. Soc.* **2020**, *40*, 4010–4015. [[CrossRef](#)]
52. Peng, Z.; Liang, P.; Wang, J.; Zhou, X.; Zhu, J.; Chao, X.; Yang, Z. Interfacial effect inducing thermal stability and dielectric response in $CdCu_3Ti_4O_{12}$ ceramics. *Solid State Ion.* **2020**, *348*, 115290. [[CrossRef](#)]
53. Moulson, A.J.; Herbert, J.M. *Electroceramics: Materials, Properties, Applications*, 2nd ed.; Wiley: West Sussex, New York, 2003; p xiv; 557p.
54. Schmidt, R.; Stennett, M.C.; Hyatt, N.C.; Pokorny, J.; Prado-Gonjal, J.; Li, M.; Sinclair, D.C. Effects of sintering temperature on the internal barrier layer capacitor (IBLC) structure in $CaCu_3Ti_4O_{12}$ (CCTO) ceramics. *J. Eur. Ceram. Soc.* **2012**, *32*, 3313–3323. [[CrossRef](#)]
55. Rahaman, M.N. *Ceramic Processing and Sintering*, 2nd ed.; M. Dekker: New York, NY, USA, 2003; p xiii; 875p.
56. Tuichai, W.; Danwittayakul, S.; Chanlek, N.; Takesada, M.; Pengpad, A.; Srepusharawoot, P.; Thongbai, P. High-Performance Giant Dielectric Properties of Cr^{3+}/Ta^{5+} Co-Doped TiO_2 Ceramics. *ACS Omega* **2021**, *6*, 1901–1910. [[CrossRef](#)] [[PubMed](#)]
57. Sangwong, N.; Somphan, W.; Thongbai, P.; Yamwong, T.; Maensiri, S. Electrical responses and dielectric relaxations in giant permittivity $NaCu_3Ti_3TaO_{12}$ ceramics. *Appl. Phys. A* **2012**, *108*, 385–392. [[CrossRef](#)]